Nanoscale deformation mechanism of TiC/a-C nanocomposite thin films

Chen, C. Q.; Pei, Y. T.; Shaha, K. P.; de Hosson, J. Th. M.

Published in:
Journal of Applied Physics

DOI:
10.1063/1.3130123

Nanoscale deformation mechanism of TiC/a-C nanocomposite thin films

C. Q. Chen, Y. T. Pei, K. P. Shaha, and J. Th. M. De Hosson[a)]
Department of Applied Physics, Materials Innovation Institute M2i, University of Groningen, Nijenborgh 4, 9747 AG Groningen, The Netherlands

(Received 29 November 2008; accepted 11 April 2009; published online 9 June 2009)

This paper concentrates on the deformation behavior of amorphous diamondlike carbon composite materials. Combined nanoindentation and *ex situ* cross-sectional transmission electron microscopy investigations are carried out on TiC/a-C nanocomposite films, with and without multilayered structures deposited by pulse dc magnetron sputtering. It is shown that by controlling the distribution of nanocrystallites forming nanoscale multilayers, the system can be used as a "microstructural ruler" that is able to distinguish various deformation patterns, which can be hardly detected otherwise in a homogeneous structure. It is shown that rearrangement of nanocrystallites and displacement of a-C matrix occur at length scales from tens of nanometer down to 1 nm. At submicrometer scale homogeneous nucleation of multiple shear bands has been observed within the nanocomposites. The multilayered structure in the TiC/a-C nanocomposite film contributes to an enhanced toughness. © *2009 American Institute of Physics*. [DOI: 10.1063/1.3130123]

I. INTRODUCTION

Diamondlike carbon (DLC) is a well established and intensively studied carbon material due to its intriguing physical properties and numerous applications based on a combination of high hardness, wear resistance, thermal stability, and electronic properties.[1] DLC based nanocomposites incorporating nanosized particles, such as carbides, nitrides, or diamond reinforcements, are expected to further improve the structural and functional properties of pure amorphous DLC materials.[2–5] However, despite the importance and extensive study on amorphous and nanocomposite carbon systems, several aspects regarding the deformation and fracture behavior at the nanoscale, and the underpinning physical mechanisms are not yet understood. Recently several molecular dynamics (MD) simulations have been reported on the deformation and fracture mechanism of DLC and DLC-based nanocomposite at atomic scale.[6–9] However, direct experimental validations of the theoretical models are not available.

High resolution transmission electron microscopy (HRTEM) is the most direct method to observe the effects of a mechanical response at nanometer scales. Nevertheless, it experiences a practical difficulty in the examination of deformed DLC or DLC-based nanocomposites due to the amorphous nature of DLC. In crystalline materials, HRTEM makes use of the fact that defects create local discontinuity in the otherwise perfect periodicity of the crystalline structure. Thus, it is the presence of a lattice acting as an intrinsic reference that allows the detailed characterization of various defects such as line defects (dislocations) and planar defects (homophase and heterophase interfaces), and to investigate their evolution during or after deformation. However, in pure DLC or a homogeneous DLC-based nanocomposite, the amorphousness and homogeneous state at various length scales make tracing of defects and nanostructure evolution during and after deformation quite elusive. In this paper we demonstrate that, by controlling the distribution of nanocrystallites (NCs) so that they form nanoscale multilayers, the NCs can serve as perfect markers for distinguishing various deformation patterns that can hardly be detected in a homogeneous structure. Multilayers with bilayer thicknesses down to <10 nm and interparticle distance of ~ 1 nm provide extremely fine interior markers for high resolution observations.

This paper concentrates on visualizing nanoscale deformation mechanisms of the nanocomposite thin films under depth sensing indentation. XTEM (cross-sectional transmission electron microscopy) investigation of individual indents on a thin film is a nontrivial problem, due to the difficulty of precisely preparing a cross-section specimen out of the microscaled indent. Although focused ion beam milling is capable of slicing TEM specimens precisely at a desired position[10–13] and had been recently used in our group for similar purpose,[10] it is found rather difficult to obtain very thin specimens suitable for high quality HRTEM observation. In this work, a special design making an array of nanoindentations (up to 400) is used and followed by classic XTEM specimen preparation. This method of XTEM specimen preparation may produce extremely thin specimen for atomic scale high resolution examination of a particular indent or even a specific area within the indent, due to the feasibility of intentional interruption and resumption of the ion beam thinning process.

In this work, the nanoscale deformation processes are first visualized in a typical nanolayered nanocomposite thin film. Thereafter, investigations are extended to nanocomposites of various structural configurations, with and without multilayer and having controlled TiC NCs size and distribution, as a follow-up of our recent letter paper.[14] An interparticle deformation process involving rearrangement of TiC NCs and displacement of a-C matrix is demonstrated to dominate the deformation mechanism at length scales rang-

[a)]Author to whom correspondence should be addressed. Tel.: +31-50-363 4898. FAX: +31-50-363 4881. Electronic mail: j.t.m.de.hosson@rug.nl.

TABLE I. Chemical composition, thin film thickness t, wavelength Λ of multilayers, volume fraction V_F, and size d of TiC particles, and mechanical properties including hardness (H), Young's modulus (E) (H and E are derived from the data with displacement up to 100 nm indentation, i.e., $<1/10$ of the film thicknesses), as well as the ratio of residual to total indentation depth d_r/d_t

Thin film	Composition (at. %)			t (μm)	Λ (nm)	V_F (%)	d (nm)	H (GPa)	E (GPa)	H/E	H^3/E^2 (GPa)	d_r/d_t (%)
	C	Ti	O									
$C_{85}Ti_{15}$	84.8	14.9	0.3	1.30	7.5	27.4	2–4	19.1	195.2	0.098	0.183	53.8
$C_{73}Ti_{27}$	71.7	27.1	1.2	1.29	11.4	52.4	3–5		207.9	0.101	0.217	51.8
$C_{65}Ti_{35}$	64.0	35.0	1.0	1.50	uniform	69.1	3–5	27.5	262.5	0.105	0.302	48.5

ing from tens of nanometers down to 1 nm. The mechanism and toughening effect of this interparticle process are discussed. This process provides a link between the submicron deformation, which can be readily experimentally revealed, and the atomic scale process as recently modeled by molecular dynamics simulations.

II. EXPERIMENTAL

The TiC/a-C nanocomposite thin films were deposited on ⟨001⟩ oriented Si wafer via a nonreactive magnetron sputtering process in a TEER UDP400/4 closed-field unbalanced magnetron sputtering system. Pulsed dc power supplies were used to power the magnetrons with graphite targets and to bias the substrate negatively. The detailed setup has been reported elsewhere.[15] In this work, a 350 kHz pulse frequency is used to enhance the impingement at the growing interface, which is critical for producing the multilayers and adjusting the configurations at proper Ti concentrations. The deposition parameters of the thin films are listed in Table I, with the thin films having three different Ti contents named according to the atomic ratio of C and Ti elements analyzed by electron probe microanalyzer. A typical substrate bias of 40 V was used for deposition.

To improve the adhesion between the thin film and the substrate, an intermediate layer of TiCr has been deposited between the substrate and the top thin film with 5.0 A and 0.4 A currents applied to Cr and Ti targets for all the thin films, respectively. Design of the composite TiCr is to introduce multilayers and to suppress the column structure growth inside the intermediate layer, where Ti is used to improve the strain accommodation and Cr to increase the hardness and elastic modulus.

Depth sensing indentation with a Berkovich diamond indenter is employed to measure the indentation hardness and modulus of the nanocomposite thin films and to study their deformation mechanism. The indentations are performed with a MTS Nanoindenter XP® system. TEM observations of the nanostructure of the top layer and interlayer were carried out before and after indentation in a JEOL 2010F HR-TEM operating at 200 kV and having an energy filtering system. Si wafer was used as a model substrate that is expected to decrease the influence of substrate because of its high modulus and hardness.[16] For postindentation XTEM investigation, a special design making an array of nanoindentations (up to 400) is used. Two indented samples were glued face-to-face, followed by cutting, grinding, dimpling, and finally ion thinned to electron transparent thickness using a Gatan PIPS operated at 3.5 kV.

III. RESULTS

A. Nanostructure and mechanical properties

With the optimized deposition parameters, nanoscale multilayers are successfully produced in the thin films $C_{85}Ti_{15}$ and $C_{73}Ti_{27}$ with well aligned TiC NCs. As shown in Fig. 1(a), the multilayers in the thin film $C_{85}Ti_{15}$ consist of amorphous carbon sublayers (bright lamellae) and Ti-rich sublayers (darker lamellae) composed of aligned discrete TiC NCs. The microstructure parameters for all the thin films are listed in Table I. The bilayer thickness and the diameter of TiC NCs increase with increasing Ti contents. Interestingly, we noticed that the multilayered structure is formed through a self organization process governed by the interdiffusion of C and Ti, with the bilayer thickness, the size of TiC NCs and interface roughness controllable with the intensity of concurrent ion bombardment but independent of substrate rotation speed. The detailed mechanism is out of the scope of this paper and will be discussed elsewhere. By increasing Ti content to $C_{65}Ti_{35}$, the whole system evolves into uniform nanocomposite of homogeneously distributed TiC nanoparticles separated by very thin a-C tissue phase (matrix) as shown in Fig. 1(c).

The indentation hardness listed in Table I shows a monotonic increase with Ti contents: from 19 GPa for the thin film $C_{85}Ti_{15}$ to 21 GPa for the thin film $C_{73}Ti_{27}$ and then rapidly rising to 27 GPa for the thin film $C_{65}Ti_{35}$. The Young's modulus shows a similar tendency of increase. The other two parameters often used to predict the wear resistance of a thin film, i.e., the ratios H/E and H^3/E^2, are also listed in Table I. The ratio H^3/E^2 is considered as an indicator of the resistance to plastic deformation in loaded contact while H/E ratio is known as the elasticity index.[17] These two ratios increase with increasing Ti content, suggesting an enhanced deformation and wear resistance of the nanocomposite thin films.

Figure 2(a) shows indentation load responses of the three thin films indented to a maximum depth of 1200 nm, which almost penetrated through the entire thin film thickness. The load-depth curves show a weak discontinuity at large indentation depths, which could be related to the phase transformation inside the Si substrate as to be discussed later. Scanning electron microscopy (SEM) top views of the

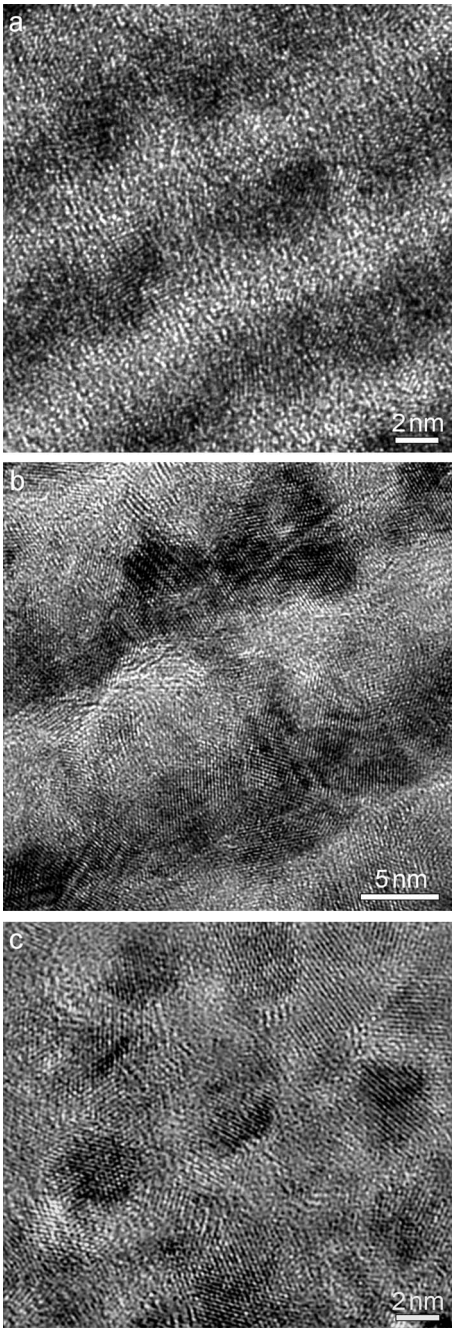

FIG. 1. High resolution XTEM micrographs showing the microstructure evolution of the coatings with increasing Ti content: multilayered structure of the coating $C_{85}Ti_{15}$ (a) and $C_{73}Ti_{27}$ (b), and homogeneous nanostructure of the coating $C_{65}Ti_{35}$ (c).

impressions confirmed no radial cracks formed along the indenter corners. Closer examination reveals only a couple of tiny and discontinuous side cracks located at the border of the impressions due to high tensile strain there, which become increasingly noticeable with increasing Ti content but are still small surface cracks even in the film $C_{65}Ti_{35}$ [Fig. 2(b)] as to be further discussed. Plastic deformation in the indented thin films may be estimated by the ratio of residual indentation depth to the total indentation depth d_r/d_t derived from the load response curves, as listed in Table I. The obtained values ranging from 48.5%–53.8% at 1200 nm indentation depth are reasonably high, which can be considered as an indication of a tough character of the nanocomposites.[18]

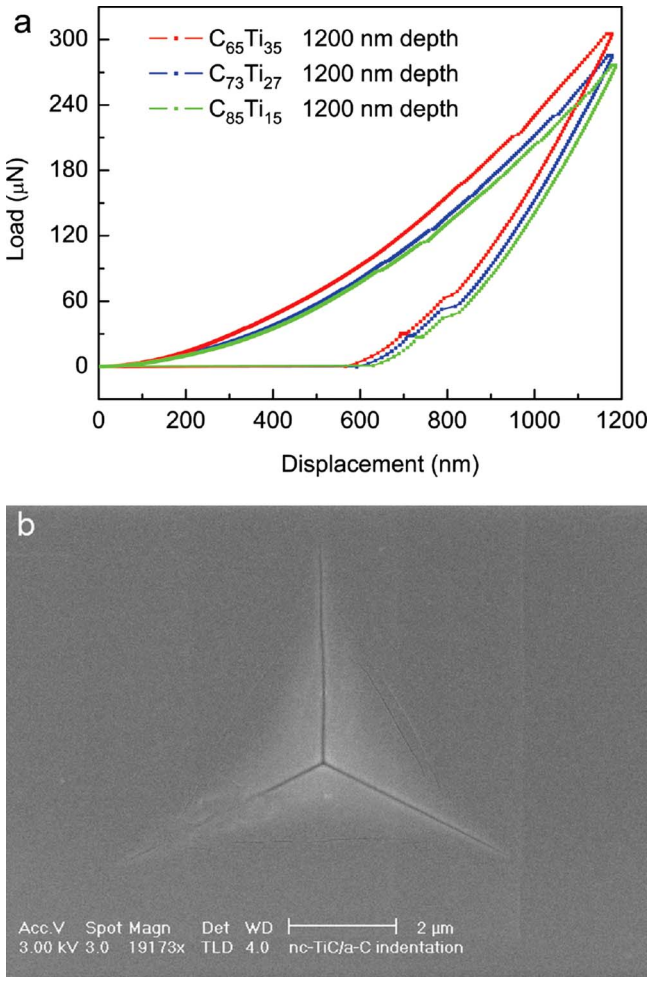

FIG. 2. (Color online) (a) Indentation load responses of three nanocomposites coatings indented to a maximum depth of 1200 nm and (b) SEM top view of an indent revealing tiny side cracks in the coating $C_{65}Ti_{35}$.

B. Visualization of deformation processes from micro- down to nanoscale

1. Thin film $C_{73}Ti_{27}$: Shear delocalization and nanocrystallites rearrangement

To make use of well aligned NCs as nanomarkers for the observation of nanoscale deformation process, the nanolayered film $C_{73}Ti_{27}$ is first examined. Deformation behaviors are examined at the indentation depth of 1000 and 1200 nm, close to the thickness of the top-layer and the entire thin film, respectively. It provides information of the deformation mechanism in the nanocomposite especially near the top layer-interlayer interface where major shear processes transfer from the interlayer to the top layer with increasing indentation depth. At both indentation depths, XTEM observations reveal no detectable cracks or delamination formed at various interfaces. Figure 3 shows the deformation morphologies of a 1000 nm deep indent in the thin film $C_{73}Ti_{27}$. It can be seen that the interlayer already shows significant plastic deformation to accommodate externally applied strain. The dark field image of the deformed interlayer in Fig. 3(c) reveals clearly two dominant and highly localized shear processes appearing symmetrically at either side of the indent, which will be further analyzed later.

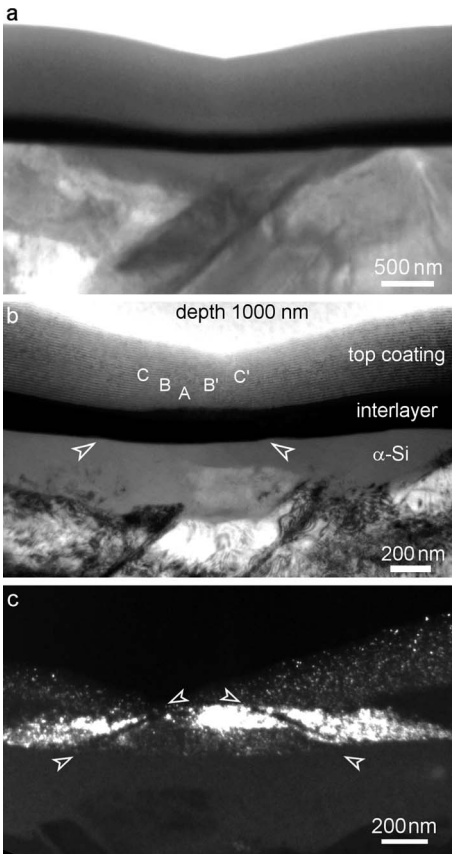

FIG. 3. XTEM micrographs showing a 1000 nm deep indent in the coating $C_{73}Ti_{27}$: (a) overall morphology, (b) magnified micrograph taken after further ion-thinning (part of the top coating removed) revealing localized plastic deformation indicated by arrows; (c) dark field image taken after ever further ion-thinning highlighting the intense SBs in the interlayer indicated with arrows.

Bright field TEM micrographs at moderate magnifications reveal that one of the common deformation morphologies of the indented top layer is the permanent bending of the sublayers following indenter tip geometry, which is necessarily accompanied by an in-plane extension [Fig. 3(b)]. At the same time, a resulting reduction of the layer spacing up to ~50% is observed underneath the indenter, which is consistent with the ratio of residual indentation depth to the total indentation depth listed in Table I. An interesting feature revealed by closer observations is the numerous shear bands (SBs) inclined at an angle of about 60° to the substrate interface and distributed symmetrically on both sides of the impression (Fig. 4). High shear deformation in an indentation is common due to the huge strain gradient, the intrinsic nature of nanoindentation. What is interesting is that many homogeneously distributed, rather than a few predominant and highly localized SBs, have been observed, the latter being the common situation in bulk amorphous materials. In addition, these multiple SBs are of short range characters, namely, propagating only several nanolayers rather than crossing the entire cross section of a thin film as shown in Fig. 4.

At 1200 nm indentation depth, the nanocomposite film shows much enhanced plastic deformation especially near the interlayer, with several highly localized major SBs distributing symmetrically on both sides of the indent. The deformation morphology is shown in Fig. 5, while a schematic illustration representing the microscale deformation features as well as the nanoscale deformation processes visualized subsequently with high resolution XTEM investigations is displayed in Fig. 6. In addition to the two central primary SBs, several new (secondary) SBs formed. The two central bands initiated from the two sharp wedges at the top side of the interlayer, which arise most likely from the lattice dislocation sliding along the $\{10\bar{1}0\}\langle 1\bar{2}10\rangle$ slip system in the interlayer.

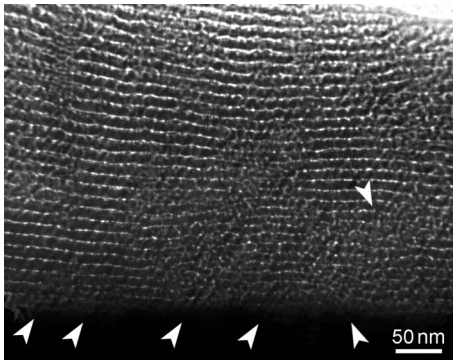

FIG. 4. Bright field XTEM image at a modest magnification showing multiple short-range shear processes within an impression of 1000 nm depth in the coating $C_{73}Ti_{27}$.

Interestingly, the abrupt shear deformation is gradually weakened by the nanocomposite multilayers after it transfers through the interlayer/toplayer interface. The two central SBs in the top layer carry the highest shear strain $\gamma = s/w$ at the interface, where they have the highest shear displacement s (height of the wedge), and the minimum width w. After crossing the interface, the abrupt SB expanded gradually to a certain width (up to ~50 nm), and the shear displacement s fades off gradually after propagating not more than 150 nm into the top layer, clearly demonstrating a shear delocalization effect of the multilayered nanocomposite (see the schematic in Fig. 6).

According to the local deformation morphologies and shear/normal strain resolved with the help of the layered nanomarkers, an impression of the multilayered nanocomposite can be roughly divided into several regions as illustrated in

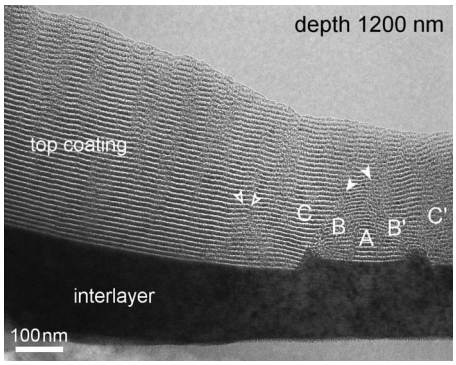

FIG. 5. Cross-sectional morphology of a 1200 nm deep indent in the coating $C_{73}Ti_{27}$, with solid arrows indicating the central major SBs and open arrows pointing to the side major SBs.

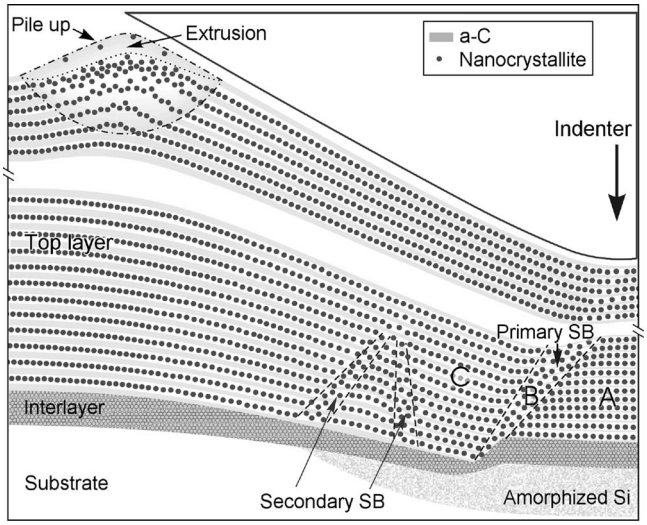

FIG. 6. Schematic illustration of submicroscale deformation morphologies and nanoscale deformation mechanism of indented multilayered nanocomposite films. The microscale features, like multilayer densification at the center, primary and secondary SBs at either side of the indent, pile up (unique for $C_{85}Ti_{15}$) at the edge, are linked to nanoscale interparticle processes, including reordering of NCs and extensive relative sliding in the nanocomposite, which are visualized by high resolution XTEM observation with the help of well aligned NCs. The multiple short-range SBs shown in Fig. 4 are excluded for better view.

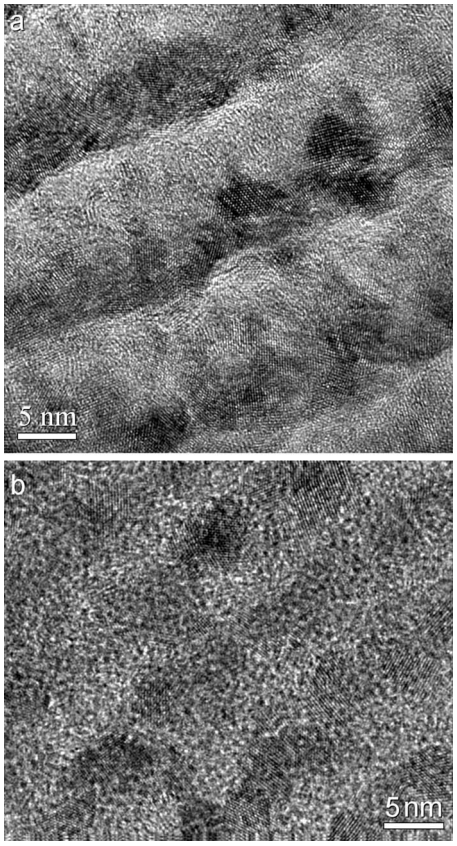

FIG. 7. Comparison of the nanostructure of the coating $C_{73}Ti_{27}$ (a) before and (b) after indentation showing densified wavelength of the multilayers in the region "A" and rearrangement of the NCs in individual Ti-rich sublayers from more than 1 monolayer into a monolayer.

Figs. 3(b), 5, and 6. The regions A, C, and C′ are dominated by normal strain and primarily characterized by layer densification, while regions B and B′ are featured by intense shear strain. Figure 7 is a comparison between the undeformed and deformed nanostructures taken from the region A. In the original multilayered nanocomposite [Fig. 7(a)], each Ti-rich sublayer contains more than one monolayer of TiC NCs such that the TiC NCs near the Ti-on-C interface almost touch each other but those near the C-on-Ti interface are more loosely distributed in a-C phase. In correspondence with the compressed wavelength of the multilayers after indentation, the particles spacing between two adjacent Ti-rich sublayers in the region A [see Figs. 2(b) and 5(b)] has been decreased noticeably [Fig. 7(b) and the schematic in Fig. 6]. That is to say, the in-plane extrusion and densification of the a-C sublayers are mainly the result of the severe indentation. In addition, the configuration of the nanoparticles in the Ti-rich sublayers also changes by means of remarkable displacements and rearrangements. Each Ti-rich sublayer after indentation is composed of a monolayer of TiC NCs well separated by the a-C phase [Fig. 7(b)]. The separation is about 1–2 nm thickness, noticeably larger than that before indentation (less than 1 nm). This kind of reconfiguration of the nanoparticles can happen only when a remarkable sliding between TiC NCs is accompanied with significantly plastic flow of the a-C matrix under the strain gradient inside the indent. The flow of the a-C matrix occurs not only in the a-C sublayers but also in the very thin intralayer regions separating the nanoparticles in the Ti-rich sublayers, resulting in an interparticle process of plastic deformation.

Within the regions B and B′ that bear intense shear strain as marked in Figs. 2(b), 5, and 6, the well-defined nanolayers become diffuse after the intensive shear deformation [Fig. 8(a) and schematically shown in Fig. 6]. Under high magnification, these regions show a homogeneous structure characterized by random and homogeneous distribution of the nanoparticles, with the particle size unchanged [Fig. 8(b)]. This indicates a relative movement of the nanoparticles following the shear deformation and mixing of the nanoparticles from adjacent Ti-rich sublayers. The random and homogeneous distribution of TiC NCs is a result of the intersection between in-plane deformation and shear banding inclined to the sublayers as indicated in Figs. 3(b) and 4. Plastic deformation has not been observed in the individual TiC NCs due to their intrinsic high strength and suppressed dislocation activity resulting from the nanometer sizes. The deformation is mainly accommodated by an interparticle-mediated process, namely, nanoparticle sliding mediated by displacement of the a-C matrix under the high strain gradient.

2. Thin film $C_{85}Ti_{15}$: Long range displacement of a-C and TiC nanoparticles

According to the above observation, it seems reasonable to expect a considerable plastic flow of the a-C matrix surrounding the TiC particle. Consequently, such a-C mediated process may be more significant in a thin film with a higher fraction of a-C matrix, e.g., the thin film $C_{85}Ti_{15}$. Figure 9(a) shows the cross-sectional morphology of a 1200 nm deep indent in the thin film $C_{85}Ti_{15}$. A clear pile up can be

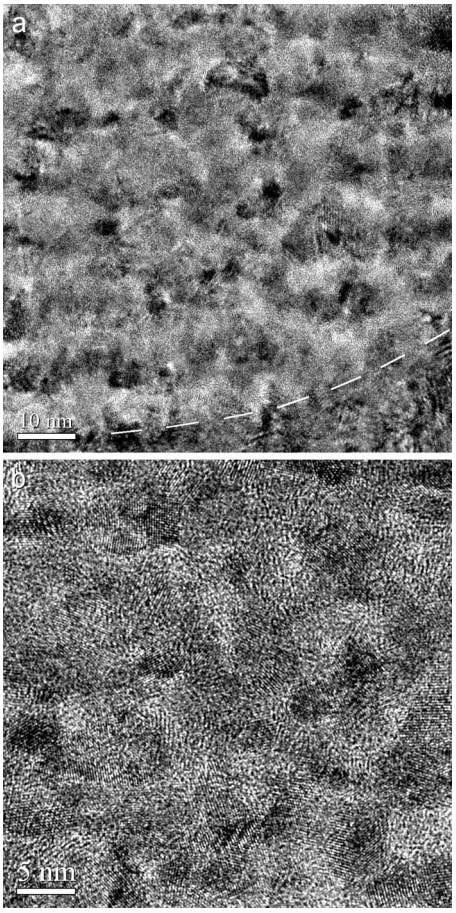

FIG. 8. (a) Diffused multilayer structure in the region B/B′ with intense shear deformation adjacent to the interlayer (note the interface bent by the intensive SBs marked with a dashed white line); (b) completely random distribution of TiC NCs as a result of particle sliding and rearrangement.

observed at the edge of the indent. Under high resolution observation, the outmost part (about 50 nm thickness) of the pile-up region shows a very bright contrast. The HRTEM micrograph reveals that this region is composed mainly of a-C embedded with very few randomly distributed TiC NCs [Fig. 9(b)], indicating a preferential squeezing of the a-C matrix to the front of the pile up as schematically shown in Fig. 6. Consequently, the very pile up front may be better understood as an outward "extrusion" of the a-C matrix under high strain gradient underneath the indenter tip. Behind the pile up front is a region composed of dense nanoparticles due to the flow of a-C matrix [Fig. 9(c)]. This process is accompanied at the same time by a rearrangement of the nanoparticles as illustrated in Fig. 6. As a result, the original multilayered structure fades off.

Compared with the above observed rearrangement of the nanoparticles in the thin film $Ti_{73}C_{27}$, the relative motion of TiC NCs and a-C matrix in the thin film $C_{85}Ti_{15}$ occur at much larger length scales (>20 nm), attributed to the increased volumetric fraction of the moving a-C matrix. Importantly, the extensive displacement and rearrangement of TiC NCs along with the a-C matrix do not lead to distinguishable cracks or nanocavities in any way. No cracks or voids are observed in the matrix or at the interfaces of a-C/TiC NCs in this thin film, with close examination confirmed atomic scale integrity at the interface.

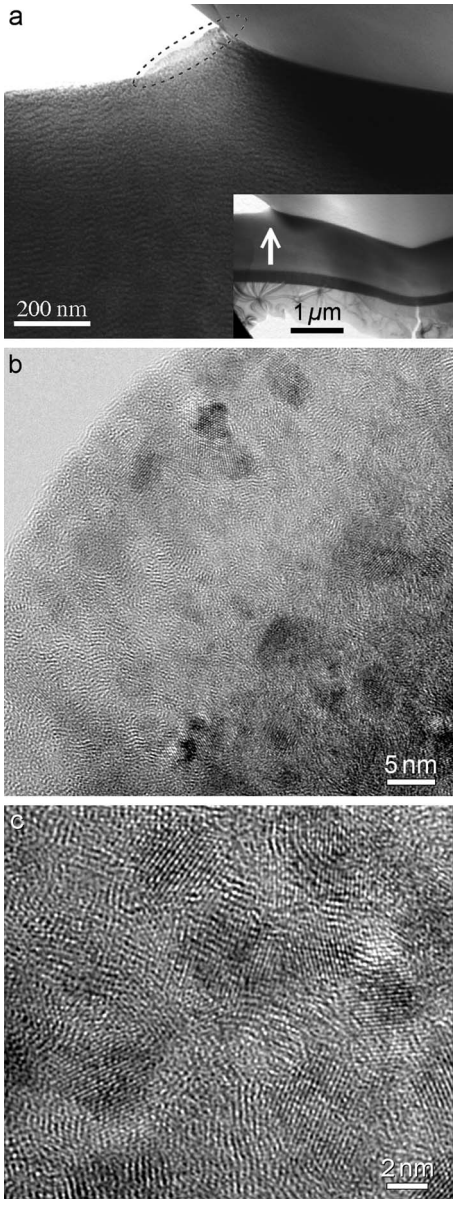

FIG. 9. Pileup at the edge of a 1200 nm deep indent in the coating $C_{85}Ti_{15}$: (a) overview, (b) the pileup front composed mainly of a-C embedded with a very few TiC NC and (c) densely packed NCs behind the pileup front due to the outflow of the a-C matrix.

Nevertheless, within the region of dense nanoparticles experiencing extensive deformation with the outflow of a-C matrix [as shown in Fig. 9(c)], direct contact between the hard particles may occur as illustrated in Fig. 6. In this case very high local contact stress may be generated and as a result, local deformation of individual particles may be possible. Deformation-induced defects, if any, could possibly be retained within the individual nanoparticles after indentation. Figure 10 shows the HRTEM micrograph of two individual nanoparticles taken from the same region as that of Fig. 9(c). Some kinds of lattice voids or cracklike defects inside these nanoparticles can be observed. Nevertheless, this kind of defects is restricted within the NCs and without propagating to the phase interface or into the surrounding matrix, and thus has a limited contribution to the deformation or fracture process.

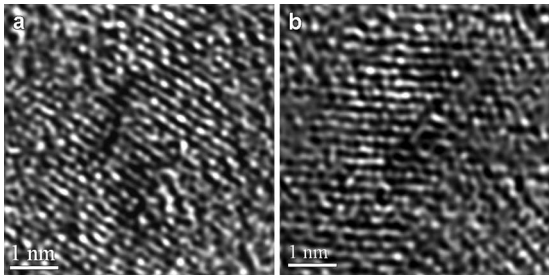

FIG. 10. HRTEM micrographs showing lattice distortion or nanocrack-type defects within individual TiC NCs.

3. Thin film $C_{65}Ti_{35}$: Advancing crack dissipated by TiC nanoparticles

In the thin film $C_{65}Ti_{35}$, the whole system is composed of homogeneously distributed TiC nanoparticles instead of multilayers with thicker Ti-rich sublayers and thinner a-C layers. The reason of this microstructure transition is related to a self organization process, which will be detailed in another paper. For such a homogeneously nanostructured system, it is hard to distinguish any deformation path/morphology regarding the interparticle deformation process due to the lack of intrinsic markers as already stressed in the introduction section. In this case, our interest focuses on possible cracks and their propagation behavior under indentation, keeping in mind the interparticle processes revealed in the multilayered nanocomposite.

As shown in Fig. 11(a), the small surface side cracks of the indent previously revealed by SEM top view [Fig. 2(b)] are observed to propagate only a very short distance (hundreds nanometer) underneath the surface. The propagating cracks follow the a-C tissue phase in-between the TiC NCs [Fig. 11(b)], and finally is halted at the nanoparticles. In addition, deflection of propagating cracks is obvious in the nanocomposite. It is very interesting that, instead of propagating continuously, the crack is halted at the TiC NCs but restarts at a region a few nanometers away from the crack tip. From the HRTEM image presented in Fig. 11(b), it seems that the crack is arrested at the left bottom by the nanoparticles and starts in a distance tens of nanometers ahead.

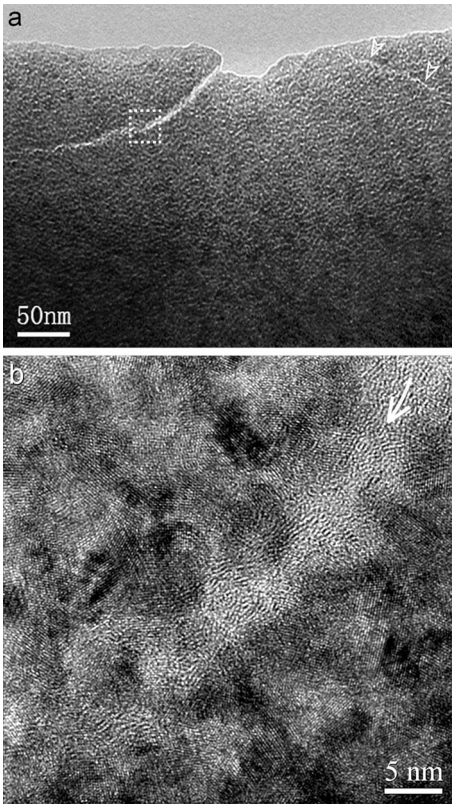

FIG. 11. XTEM micrographs showing restrained micro-/nanocracks in an indent in the coating $C_{65}Ti_{35}$: (a) overview and (b) magnified HR-XTEM micrograph taken from the area marked with a square box in (a).

Under indentations up to a depth of 1200 nm that is close to penetrating the entire thin film thickness, all three thin films show excellent structural cohesion at various interfaces, without cracks, microvoids, or delamination detected. The interlayer was found to perform very well in accommodating the plastic deformation and to keep the interface adhesion. Another factor contributing to the perfect adhesion at the substrate-thin film interface is dislocation slip and phase transformation plasticity of the Si substrate,[19,20] which was clearly observed under the applied large indentation depth even penetrating into the Si substrate. The slight pop-in and distinct pop-out appear to be due to the slip and transformation in the silicon,[19] as they are observed even for thin films without any cracking or delamination detected.

IV. DISCUSSION

A. Mechanism of interparticle process and flaw tolerance at nanoscale

One of the major phenomena observed in the present work is the extensive interparticle process characterized by rearrangement of TiC NCs and remarkable a-C displacement at nanometer scale as schematically illustrated in Fig. 6. This a-C matrix assisted process becomes increasingly significant in the thin films of higher volumetric fraction of a-C matrix, provided the distance between the NCs is comparable with their size.[2] Within individual TiC nanoparticles, general plastic deformation was not observed due to the intrinsic high strength of TiC and suppressed dislocation activities at nanometer size. To accommodate the interparticle process, besides particle translation, grain (particle) rotation is considered as another favorable mechanism involved in the rearrangement of nanoparticles. Although it has not been directly distinguished with XTEM on individual NCs due to the amorphous nature of the a-C matrix, this grain rotation mechanism has been proven to be one of the major deformation mechanisms in nanocrystalline materials.[21] Extensive displacement of a-C has been observed either in the a-C sublayer separating the Ti-rich layers or the a-C tissue phase within individual Ti-rich layers. The most interesting observation is that even with extensive displacement and relative sliding under large deformation, observable cracks and cavities can be successfully avoided either at the boundaries between the various layers in the multilayered structure or the phase boundaries between TiC and a-C.

HRTEM confirmed the atomic scale integrity at the phases boundary, i.e., the interface between a-C matrix and

TiC NCs, without detectable nucleation and coalescence of voidlike defects [Figs. 7(b) and 8(b)] even in the area experienced significant out flow of the a-C matrix [Fig. 9(c)]. Considering the extensive relative sliding, it seems reasonable to assume that the bonding either at the interface or within the a-C has the capability to re-establish the bond after it was broken. Recently MD simulations[7] on a-C embedded with diamond crystallites suggested the possibility of bond breaking and reattaching at the interface of a-C and hard particles during the process of relative sliding at the interface, which seems in a good agreement with our HR-TEM experimental observation.

Apart from the behavior at the phases interface, atomic sliding in the a-C itself is necessary to achieve the interparticle process and large displacement of a-C [e.g., that shown in Fig. 9(b)] while keeping the bonds undestroyed. The amorphous structure of DLC containing mainly sp^2 bonded carbon seems to favor the interparticle sliding and a-C displacement, which could be further improved by doping of Ti.[22] However, the atomic scale deformation process in a-C matrix related to the sp^2/sp^3 ratio has not been well understood up to now.[6,7] Microscopic quantification of the effects of sp^2 fraction in the a-C on the interparticle process is still a challenge but in the present case the sp^2 dominates over sp^3.

In a recent MD simulation,[9] the amorphous based nanocomposites have been reported to exhibit a certain flaw tolerance. That is to say, fracture is a gradual process accompanied by gradual nucleation and coalescence of voidlike defects and especially, cracklike defects smaller than 40 Å have almost no effect on the fracture strength. This flaw tolerance for fracture in amorphous carbon appears to be due to its intrinsic structure disorder. Therefore, flaw tolerance may be a characteristic of disordered atomic structures at the nanoscale.

B. Mechanism of toughening regarding the nanoscale interparticle process

The collective behavior of the interparticle process operating at nanometer scale has significant effect on the structural response at modest (medium) length scales, and prompts shear delocalization in nanocomposite thin films. The nanocomposites are composed of two kinds of phases, i.e., TiC NCs and highly disordered/amorphous a-C. The deformation behaviors of the nanocomposites are found being distinct from that of either nanocrystalline[23] or bulk amorphous materials,[24] and the latter suffer highly localized shear banding often resulting in catastrophic failure.

In the nanocomposites, shear deformation occurred in the amorphous matrix can be tuned by the existence of the NCs, evolving interparticle process, and assisted by the flow of a-C matrix. As a result, a large number of short-range multiple SBs nucleate homogeneously throughout the specimen and carry uniform shear deformation. The three dimensional a-C matrix seeds the initiation of organized SBs and confines them to small domains, i.e., the a-C sublayers and interparticle boundary regions. The nanoparticles and TiC-containing sublayers act as obstacles to restrict excessive deformation in these domains. In this way, shear deformation becomes effectively delocalized. The flaw tolerance enables the a-C matrix to sustain reasonable shear deformation without causing catastrophic failure. Even when SBs carrying extremely high shear strains occur in the interlayer, they can be delocalized in the top layer by flowable a-C carrying TiC nanoparticles and consequently the shear strain fades away after the SBs travel a small distance.

The toughening mechanism for the nanocomposite thin films is consistent with the previously proposed ideas of composite microstructure for bulk amorphous alloys[25] and recently for nanocrystalline metals.[26] Another toughening mechanism in the nanocomposite thin film is to dissipate propagating cracks via confinement in the a-C tissue phase. Micro-openings are surfaced by NCs [Fig. 11(b)] that substantially increase surface area and surface energy that has to be overcome for the crack to propagate. This is confirmed by the fact that the crack does not continuously propagate, but is repeatedly halted and restarts at an area ahead of the crack tip, as clearly indicated by the indicated individual cracks. This crack reinitiation together with the deflection effect essentially causes a reduction in the crack-driving force or stress intensity factor and consequently increases the fracture toughness. A detailed analysis on these effects based on fracture mechanic analysis can be found in Refs. 27 and 28.

V. CONCLUSIONS

Well aligned NCs that form multilayers serve as extremely fine intrinsic markers in XTEM to reveal the deformation process in TiC/a-C nanocomposite thin films subjected to nanoindentation. It is shown that by controlling the distribution of NCs forming nanoscale multilayers, the system becomes a "microstructural ruler" that is able to distinguish various deformation patterns, which can be hardly detected otherwise in a homogeneous structure. Interparticle processes, including rearrangement and sliding of TiC NCs with respect to the a-C matrix, were found to occur at various length scales (from 1 nm to tens of nanometers), assisted by the flow of the a-C matrix. Because of the nanoscaled geometric constraint, shear deformation was brought under control by multiple SBs, with each band contributing to plastic deformation but propagating only in nanometer scales and conveying a shear strain not large enough to cause local damage. At large indentation depths, the multilayered nanocomposites may delocalize abrupt shear deformation arising from the interlayer significantly. Consequently, the multilayered nanocomposite thin films exhibit a prominent plasticity while maintaining high hardness. In the nanocomposite thin film without multilayer structure, the cooperative deformation of NCs was found to dissipate and deflect propagating cracks effectively. The observed interparticle deformation mechanism facilitated by the separating a-C phase and the crack dissipation effect provide useful clues for the design of nanocomposites composed of hard NCs and a compliant amorphous matrix.

ACKNOWLEDGMENTS

This research was carried out under the project number MC7.06246 in the framework of the research program of the Netherlands Materials Innovation Institute (M2i), the former

Netherlands Institute for Metals Research, Delft, the Netherlands. The authors acknowledge financial support from the M2i and the Foundation for Fundamental Research on Matter (FOM-Utrecht), the Netherlands.

[1]J. Robertson, Mater. Sci. Eng. R. **37**, 129 (2002).
[2]Y. T. Pei, D. Galvan, and J. T. M. De Hosson, Acta Mater. **53**, 4505 (2005).
[3]A. Cavaleiro and J. T. M. De Hosson, *Nanostructured Coatings* (Springer, New York, 2006).
[4]A. A. Voevodin and J. S. Zabinski, Thin Solid Films **370**, 223 (2000).
[5]S. Veprek and S. Reiprich, Thin Solid Films **268**, 64 (1995).
[6]M. G. Fyta, I. N. Remediakis, P. C. Kelires, and D. A. Papaconstantopoulos, Phys. Rev. Lett. **96**, 185503 (2006).
[7]S. Namilae, B. Radhakrishnan, and G. B. Sarma, Compos. Sci. Technol. **67**, 1302 (2007).
[8]I. N. Remediakis, M. G. Fyta, C. Mathioudakis, G. Kopidakis, and P. C. Kelires, Diamond Relat. Mater. **16**, 1835 (2007).
[9]Q. Lu, N. Marks, G. C. Schatz, and T. Belytschkol, Phys. Rev. B **77**, 014109 (2008).
[10]D. Galvan, Y. T. Pei, and J. T. M. De Hosson, Surf. Coat. Technol. **200**, 6718 (2006).
[11]S. J. Lloyd, A. Castellero, F. Giuliani, Y. Long, K. K. McLaughlin, J. M. Molina-Aldareguia, N. A. Stelmashenko, L. J. Vandeperre, and W. J. Clegg, Proc. R. Soc. London, Ser. A **461**, 2521 (2005).
[12]S. J. Suresha, S. Math, V. Jayaram, and S. K. Biswas, Philos. Mag. **87**, 2521 (2007).
[13]J. M. Molina-Aldareguia, S. J. Lloyd, M. Oden, T. Joelsson, L. Hultman, and W. J. Clegg, Philos. Mag. A **82**, 1983 (2002).
[14]C. Q. Chen, Y. T. Pei, K. P. Shaha, and J. T. M. De Hosson, Appl. Phys. Lett. **92**, 241913 (2008).
[15]Y. T. Pei, C. Q. Chen, K. P. Shaha, J. T. M. De Hosson, J. W. Bradley, S. A. Voronin, and M. Čada, Acta Mater. **56**, 696 (2008).
[16]R. Saha and W. D. Nix, Acta Mater. **50**, 23 (2002).
[17]Y. T. Pei, P. Huizenga, D. Galvan, and J. T. M. De Hosson, J. Appl. Phys. **100**, 114309 (2006).
[18]S. Zhang, D. Sun, Y. Q. Fu, and H. J. Du, Surf. Coat. Technol. **198**, 74 (2005).
[19]A. J. Haq, P. R. Munroe, M. Hoffman, P. J. Martin, and A. Bendavid, Thin Solid Films **516**, 267 (2007).
[20]J. Neidhardt, C. Walter, J. M. Molina-Aldareguia, M. Herrmann, W. J. Clegg, and L. Hultman, J. Appl. Phys. **103**, 123515 (2008).
[21]Z. W. Shan, E. A. Stach, J. M. K. Wiezorek, J. A. Knapp, D. M. Follstaedt, and S. X. Mao, Science **305**, 654 (2004).
[22]S. Zhang, X. L. Bui, X. T. Zeng, and X. M. Li, Thin Solid Films **482**, 138 (2005).
[23]F. Spaepen, Acta Metall. **25**, 407 (1977).
[24]E. Ma, Scr. Mater. **49**, 663 (2003).
[25]C. C. Hays, C. P. Kim, and W. L. Johnson, Phys. Rev. Lett. **84**, 2901 (2000).
[26]G. He, J. Eckert, W. Loeser, and L. Schultz, Nature Mater. **2**, 33 (2003).
[27]K. T. Faber and A. G. Evans, Acta Metall. **31**, 565 (1983).
[28]J. W. Hutchinson, Acta Metall. **35**, 1605 (1987).